Geodesy and Geodynamics 2011,2(3):24 - 30

http://www.jgg09.com
Doi:10.3724/SP.J.1246.2011.00024

Co-seismic deformation of 2011 *M*w9.0 Japan earthquake observed by InSAR technique

Shen Qiang and Tan Kai

Institute of Seismology, China Earthquake Administration, Wuhan 430071, *China*

Abstract: Co-seismic line-of-sight displacements of the 2011 *M*w9.0 Japan earthquake derived from InSAR data of Envisat ASAR, ALOS PALSAR and TerraSAR-X show a maximum value of about -245cm to -221cm near the epicenter. This result is in good agreement with the result of GPS measurement. The observed displacement pattern suggests an earthquake-rupture zone over 500km long, with a ground-motion pattern in the vicinity of the northern segment more complex than that of the southern segment, possibly due to immediate aftershocks that occurred between satellite passes.

Key words: *M*w9.0 Tohoku earthquake; InSAR; surface displacement

1 Introduction

A catastrophic *M*w9.0 earthquake occurred on March 11, 2011 at a depth of 32 km in western Pacific Ocean, approximately 72 km east of Japan[1]. In this paper, we report on a study of the co-seismic deformation field based on InSAR radar images from Envisat ASAR, ALOS PALSAR and TerraSAR-X, covering areas shown in figure 1. We then compared our preliminary result with the result of GPS measurement for verification.

2 Data and processing

Several pairs of pre- and post-earthquake radar images of Envisat ASAR, ALOS PALSAR and TerraSAR-X were used to generate interferometric patterns. The surface displacements in line of sight (LOS) were obtained by using two-pass and three-pass methods, respectively.

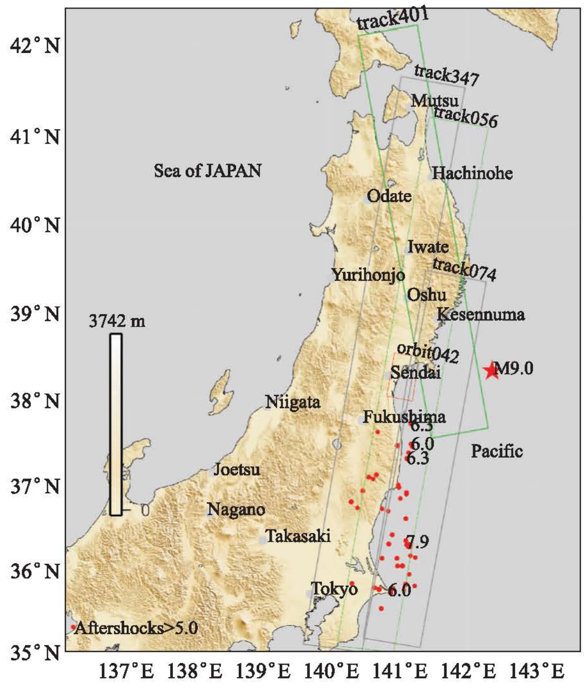

Figure 1 Locations of the earthquake epicenters, and areas covered by radar images used in this study (rectangles; Envisat in gray, ALOS in green and TerraSAR-X in red)

Received:2011-04-10; Accepted:2011-06-29

Corresponding author: +86 - 18971407030; E-mail: cl980606@hotmail.com

This work is supported by the National Natural Science Foundation of China(41004008), Key Foundation of Institute of Seismology, China Earthquake Administration (IS201026019), State Key Laboratory of Cryospheric Sciences, Cold and Arid Regions Environment and Engineering Research Institute, Chinese Academy Sciences (SKL CS09 - 03); the Foundation of State Key Laboratory of Water Resources and Hydropower Engineering Science, Wuhan University (2009B54); the Director Foundation of Institute of Seismology, China Earthquake Administration (IS200826057)

The basic parameters of interferometry are listed in table 1. Previous studies have shown that shorter spatial and temporal baselines should be used[3]. However, available radar images were very few at the time of this earthquake, and they were mainly for emergency observations. As shown in table 1, Envisat ASAR had the best temporal baseline, and ALOS PALSAR pairs had a larger valid perpendicular baseline. To illustrate the capability of TerraSAR-X, post-earthquake images with an interval of 11 days were used to compare with the co-seismic displacements.

We used the open source InSAR software ROI_PAC to process Envisat ASAR and ALOS PALSAR data with two-pass D-InSAR, the open-source software Doris to process co-seismic deformation measurements of TerraSAR-X with three-pass method, and the SARScape software to process post-earthquake displacement measurements. Key steps of processing included decoding, automatic matching, interferogram formation, topography removal, phase unwrapping, and geographic projection. Since precise orbital information was not available and the available images were taken mostly in emergency, we had to rely on the lower-accuracy prediction orbits for D-InSAR processing. This might have caused error in the calculation of the initial offset values and led to processing problems in obtaining interferometric images. Thus in the InSAR processing we needed to exercise step-by-step control, especially in image matching.

3 InSAR displacement fields and analysis

The co-seismic deformation fields from two pairs of Envisat ASAR interferometric images are shown in figure 2. The maximum LOS displacement in the area covered by track 347 was −245 cm at (141.245°E, 38.464°N) (see also top part of Fig. 3), in Ishinomaki close to the epicenter. The maximum LOS displacement in the area covered by track 074 was −221 cm at (140.994°E, 37.674°N) (see the lower part of Fig. 3), only 30 km away from the first nuclear power plant in Fukushima (TEPCO in Fig. 3), where the displacement was as high as 200 cm. Track 074, unlike track 347, revealed two areas of larger deformation, and the displacement in the southern region was generally 10 cm larger, perhaps because it was closer to the larger aftershocks. This may be seen in the GPS displacement maps also (Figs. 6 and 7).

To assess measurement precision, we first compared the above-mentioned two sets of results along a profile shared by both track 347 and track 074 (red line in Fig. 2). As shown in figure 2(c), the displacement profiles are nearly parallel with a correlation coefficient of 0.997. Figure 2 (d) shows the difference between the profiles and a polynomial fit. The difference varies from 50 cm to 70 cm, and the overall difference was mainly caused by the selected reference point for phase unwrapping, which can be eliminated through systematic correction. Additional causes include differences in satellite orbit, topography, satellite-to-ground geometry, atmosphere and temporal span, among which the effects from orbital accuracy, satellite-to-ground geometry and topography are nonlinear. Thus, it may be better to use the polynomial fit to eliminate the uncertainty caused by these satellite parameters. By using a 4-order polynomial fitting the R-square test reached 0.859, indicating that the model represents the variation of displacement difference quite well. Most of the residues in the difference are less than 5 cm, indicating a good agreement.

Table 1 Basic interferometric parameters ($B_\perp$ denotes valid perpendicular baseline)

Orbit	Sensor	Temporal span	Temporal baseline (days)	$B_\perp$ (m)
347	Envisat ASAR	2011-02-19—2011-03-21	32	−119.5
074	Envisat ASAR	2011-03-02—2011-04-01	30	−103.0
401	ALOS PALSAR	2010-10-28—2011-03-15	139	1437.5
056	ALOS PALSAR	2010-11-20—2011-04-07	139	1137.3
042	TerraSAR-X	2010-10-20—2008-09-21	759	−91.9
042	TerraSAR-X	2010-10-20—2011-03-12	143	48.1
042	TerraSAR-X	2011-03-12—2011-03-23	11	27.5